Construction and Building Materials 509 (2026) 145242

Contents lists available at ScienceDirect

Construction and Building Materials

journal homepage: www.elsevier.com/locate/conbuildmat

Corrosion behavior of bare and galvanized steel in alkali-activated and ordinary Portland cement-based mortars at the same strength class exposed to carbonation

Alessandra Mobili [a,*], Chiara Giosuè [a], Tiziano Bellezze [a], Francesca Tittarelli [a,b]

[a] Department of Materials, Environmental Sciences and Urban Planning (SIMAU), Università Politecnica delle Marche – INSTM Research Unit, Ancona 60131, Italy
[b] ISAC – CNR, Via Piero Gobetti 101, Bologna 40129, Italy

ARTICLE INFO

Keywords:
Corrosion
Carbonation
Reinforcements
Alkali-activated binders
Geopolymers
Cement
Fly ash
Metakaolin
Galvanized steel
Reinforced concrete

ABSTRACT

This study compares the corrosion behavior of bare and galvanized steel reinforcements in cement and alkali-activated mortars based on fly ash and metakaolin after carbonation. Each mortar type belonged to three different strength classes: R1 ($R_c \geq 10$ MPa), R2 ($R_c \geq 15$ MPa), and R3 ($R_c \geq 25$ MPa), and has been tested during wet/dry cycles in tap water following exposure to a 3 vol% CO_2 environment. Results in terms of electrochemical tests and visual and metallographic analysis showed that steel reinforcements corroded less in fly ash-based mortars, thanks to their low porosity (spanning for 13–19 %) and high alkalinity, with pH values stable between 13 and 14 also after accelerated carbonation. For galvanized steel, the lowest consumption of the zinc coating (up to 40 μm in cement-based matrices) was observed in metakaolin-based mortars (less than 20 μm) since the combination of low alkalinity (with pH falling between 12.5 and 11.5) and high total porosity (around 35 %) of the matrix facilitate the penetration of oxygen and CO_2 which promote the formation of a passivating layer. The significant lower susceptibility to corrosion of galvanized steel compared to bare steel resulted in this work, regardless of the binder type, suggests that the use of galvanized steel is recommended in structures exposed to carbonation not only in cement but also in alkali-activated matrices.

1. Introduction

The "safety" of reinforced concrete structures is highly influenced by the durability of building materials [1,2]. In particular, during the service life of mortars/concretes, carbonation is a critical issue, especially in warm and humid environments [3]. In cement-based materials, the carbonation process is a well understood phenomenon: atmospheric CO_2 penetrates the cement paste and reacts with $Ca(OH)_2$, forming calcium carbonate. Consequently, the pH, initially around 13 due to the saturated $Ca(OH)_2$ solution in the pores, decreases to lower values, sometimes even below 9, which is generally considered the upper pH limit for the initiation of steel rebars depassivation [4]. Then, in the presence of moisture and oxygen, corrosion can propagate.

But what happens to steel reinforcements when they are embedded in novel materials based on alkali-activated binders?

Alkali-activated materials (AAMs) are gaining attention as potential substitutes for ordinary Portland cement (OPC)-based materials due to their environmental benefits, such as lower consumption of natural resources in the production and reduced global warming impacts [5–7]. AAMs are obtained through the chemical reaction of an aluminosilicate precursor with an alkaline activator. The most commonly used precursors include ground granulated blast furnace slag (GGBFS), fly ash (FA), and calcined clays (such as metakaolin (MK)), whereas activators typically consist of alkali silicates, carbonates, and hydroxides [8]. When precursors have a low CaO content, AAMs fall under the category of geopolymers [9]. AAMs have demonstrated satisfactory mechanical performance for building applications; however, their long-term durability, particularly in terms of carbonation resistance and related reinforcement corrosion, has been addressed in the literature only recently, with most studies focusing on alkali-activated slag (AAS) [10–12] instead on alkali-activated fly ash (AAFA) or alkali-activated metakaolin (AAMK).

Kraft et al. [13] reported that on the basis of hydration products, binders can be classified into three clusters, affecting also their carbonation behavior:

* Corresponding author.
E-mail address: a.mobili@univpm.it (A. Mobili).

https://doi.org/10.1016/j.conbuildmat.2026.145242
Received 25 September 2025; Received in revised form 10 January 2026; Accepted 12 January 2026
Available online 14 January 2026

- Cluster 1 comprises binders which form calcium-silicate hydrate (C-S-H) phases and significant amounts (> 20 %) of portlandite ($Ca(OH)_2$) by hydration and do not exhibit any accelerated carbonation at 0.3 vol% CO_2. This is the cluster where OPC-based materials lie.
- Cluster 2 includes binders which form C-S-H phases but little to no portlandite by hydration and show an acceleration at 0.3 vol% CO_2, which is smaller than the acceleration at 1.0 vol% CO_2. In this cluster are comprised binders based on OPC partially substituted by calcined clays or high amount of GGBFS.
- Cluster 3 involves binders which do not form C-S-H phases and portlandite by hydration but sodium and/or potassium aluminosilicate hydrates (N(K)-A-S-H) and ettringite and undergo rapid carbonation regardless of CO_2 concentration. This is the cluster that comprises calcium sulfoaluminate (CSA) cement and AAMs. Indeed, the pore solution of AAMs contains higher concentrations of silica, aluminum, OH^- and Na^+ ions but lower concentrations of Ca^{2+} and K^+ compared to that of OPC [14].

Upon carbonation, a reduction in alkalinity has been observed in both AAMs and OPC binders, but generally AAMs have a lower CO_2-binding capacity, resulting in faster carbonation front progression compared to OPC [15–18], confirming the results of Kraft et al. [13]. In AAMs, carbonation occurs in two primary stages [19]: (1) carbonation of the pore solution, which leads to a reduction in pH and the precipitation of Na-rich carbonates, and (2) decalcification of Ca-rich phases and secondary products present in the system. This indicates that, unlike OPC-based materials, the CO_2-binding capacity of AAMs depends not only on the CaO content but also on the amount of Na_2O consumed by the reaction of precursors such as FA and GGBFS. Additionally, since the pore solution in AAMs is typically dominated by Na^+ ions, the CO_2 concentration significantly influences the carbonate/bicarbonate equilibrium in the pore solution, which in turn buffers its pH [3]. Such effects are not observed in OPC, where the carbonation process is primarily driven by calcium carbonate formation without a significant influence by soluble alkali carbonates. Specifically, in low-calcium AAMs, such as Class F FA-based AAMs and AAMK [3,20], the pH of the system is controlled solely by the sodium- and potassium-rich pore solution with a greater reduction in pH compared to high-calcium AAMs, such as AAS [21]. In high-calcium AAMs, carbonation leads to the decalcification of C-A-S-H gels and the formation of carbonates/bicarbonates such as calcite ($CaCO_3$), natron ($Na_2CO_3 \bullet 10\ H_2O$), thermonatrite ($Na_2CO_3 \bullet H_2O$), nahcolite ($NaHCO_3$), and trona ($Na_3H(CO_3)_2$) [3]. Since the formed sodium carbonates are water-soluble, this results in a decrease in mechanical strength [22] and increase in porosity [23,24], accelerating the carbonation process [23,25,26].

Research on the corrosion behavior of rebars in carbonated AAMs, particularly for metakaolin-based AAMs [16,18,27], is really still very limited and again more focused on AAS.

According to Tian et al. [28], high-calcium AAS mortars provide a better protection against corrosion than OPC counterparts but poorer performance after complete carbonation. Sufian Badar et al. [20] found that in high-calcium AAFA, carbon steel rods are poorly protected due to the high permeability of the paste, which allows significant CO_2 penetration. According to Xu et al. [14], the high concentration of sulfur species in the pore solution of AAS delays the formation of a passive film on the surface of reinforcing steel due to oxygen depletion and the competitive adsorption of sulfide at the steel surface. Furthermore, since in AAMs the formation of $Ca(OH)_2$ cannot occur, as above-mentioned, there is not an alkaline reservoir and therefore the loss of alkalinity in AAMs caused by carbonation is difficult to replenish [29].

Generally, low-calcium AAMs as geopolymers appear more vulnerable to carbonation and thus to reinforcement corrosion compared to OPC-based materials [30]. Low-calcium AAFA significantly lack of portlandite, which typically provides a buffering effect in the concrete pore solutions to maintain high pH values during carbonation; therefore, the reduced alkalinity of the pore solution caused by carbonation leads to steel passivity loss and generalized corrosion [31]. However, the resistance to carbonation and the corrosion of embedded reinforcements appear to improve with the addition of slag to a fly ash mix [32]. Nevertheless, in low-strength, low-calcium AAFA concretes, no signs of reinforcement depassivation have been reported after 500 days of exposure to a 1 % CO_2 environment [33]. According to Xu et al. [14], in carbonated low-calcium AAMs, the primary factor contributing to the depassivation of steel reinforcement is the pH drop and in simulated pore solutions high concentrations of CO_3^{2-}/HCO_3^- (carbonate/bicarbonate) ions help to mitigate this process.

The carbonation resistance of AAMs can be enhanced through various strategies, such as using retarders [17], increasing the NaOH content in the activator solution [24,34], increasing the content and fineness of GGBFS in the precursor [35], adding calcined hydrotalcite (C-HT) to promote alkali-activation [36], or incorporating sodium citrate as an environmentally friendly corrosion inhibitor [31]. However, if in the pore solution of AAMs a high pH level positively affects the generation rate and thickness of the passive film, an extremely high pH level (>13) can hinder the formation of this passive film [14].

Hot-dip galvanization of steel rebars is one of the most widely used, cost-effective methods for controlling corrosion in reinforced concrete structures (RCS) exposed to carbonation [37]. In low-calcium AAMs, the limited availability of Ca^{2+} ions could affect galvanized steel corrosion not only in terms of pH of the pore solution but also of the composition of the passivating zinc layer since, unlike bare steel, Ca^{2+} plays a significant role in zinc passivation [38]. However, there are still few studies on the behavior of galvanized steel reinforcements in AAMs under accelerated carbonation. Low-calcium AAFA appear to protect reinforcement against corrosion better than cement-based matrices [39]. On the other hand, AAMK exhibit faster carbonation than cement-based matrices, although similar polarization resistance values of rebars have been recorded during wet/dry cycles in tap water [18].

The literature provides still limited data concerning the effect of carbonation on reinforced low-calcium AAMs, which has contributed to hinder a broader application of AAMs in engineering practice nowadays [40]. While these studies are especially related to bare steel reinforcements, those concerning galvanized steel can count on the fingers of one hand. Moreover, only few studies compare the effect of natural and accelerated carbonation on the alkali-activated matrix. Therefore, this paper explores the evolution of OPC and AAMs pH during both natural and accelerated carbonation and compares the corrosion behavior induced by carbonation in both bare and galvanized steel rebars embedded in low-calcium AAFA and AAMK, with that of cement-based mortars at the same strength class. As previously reported for chloride induced corrosion [27], for each binder three different mortars were produced: two non-structural classes (R1 with $R_c \geq$ 10 MPa and R2 with $R_c \geq 15$ MPa), and one structural class (R3 with $R_c \geq 25$ MPa), according to UNI EN 1504–3. After accelerated carbonation, the reinforced mortars were subjected to weekly wet/dry cycles in tap water and the corrosion behavior of bare and galvanized steel rebars in the different matrices was investigated by electrochemical and visual/metallographic tests.

2. Experimental

2.1. Materials and mixtures proportions

Mortar mixes were prepared with the same materials and compositions already studied in a previous work [27]. Specifically, a total of 12 mortars mixes divided into 4 different groups, each one satisfying 3 mechanical strength classes (i.e., R1, R2 and R3) were studied as follows:

- group 1) CEM mixes prepared with CEM II/A-LL 42.5 R (Colacem S.p.A.) and hydraulic lime UNI 10892 LIC 3.0 (Italcementi S.p.A.);

- group 2) FANa mixes prepared with class F fly ash (General Admixture S.p.A.) activated by NaOH and sodium silicate solutions;
- group 3) FAK mixes prepared with class F fly ash and calcium aluminate cement (Kerneos Inc.) activated by KOH and sodium silicate solutions;
- group 4) MKK mixes prepared with MetaStar® 501 metakaolin (Imerys Minerals Ltd.) activated by KOH and sodium silicate solutions.

The different types of activators were chosen in order to investigate the possible effect on mechanical, physical, and durability properties of mortars and presented in a previous paper [41]. Here, it was found that the use of KOH instead of NaOH should be preferred to reduce efflorescence and to produce mortars resistant to sulfate attacks. To achieve the 3 different strength classes, CEM mixes were prepared by varying the content of hydraulic lime and the water/cement (w/c) ratio. Conversely, in AAMs the 3 different strength classes were reached by varying the concentration of NaOH and KOH solutions. All mortars were prepared with calcareous sand (Esincalce S.r.l.) and a sand/binder ratio of 3 by mass. After mixing all the ingredients, mortars were poured into molds of various geometries, depending on the specific test, and cured at $>$ 95 % relative humidity (RH) and 20 $\pm$ 1 °C temperature (T) for the first week, and then at 50 $\pm$ 5 % RH and 20 $\pm$ 1 °C until testing, unless otherwise specified.

2.2. Methods

2.2.1. Mechanical and microstructural analyses of mortars

The mortar compressive strength (R_c) was measured after 28 days of curing on 40 mm $\times$ 40 mm $\times$ 160 mm specimens, following UNI EN 1015–11. The pore microstructure was investigated on small mortar samples (approximately 1 cubic cm, one sample per mortar type) after 28 days of curing by using a Thermo Fisher 240 Pascal mercury porosimeter.

2.2.2. Paste alkalinity

In AAMs, the paste alkalinity can decrease not only through carbonation, as for cement-based matrices, but also as a result of the polymerization reaction itself [42]. To better correlate the corrosion results with the alkalinity of different mortars, for each mortar, the pH was measured at 5–15 mm, 15–25 mm, and 25–35 mm depths in unreinforced cubic specimens (100 mm per side) by drilling the center of each face. The resulting powder (approximately 5 g) was mixed with 5 ml of demineralized water to maintain a powder-to-water ratio of 1:1 by mass [43,44]. The suspension was stirred for 2 h at room temperature, and then the pH was measured with a pH-meter [27]. Each reported pH value is the averaged value obtained by three measurements [45], the differences between each set of three measurements differs less than 5 %.

For each mix (Table 1), three specimen types (S1, S2, S3) were prepared and cured according to the procedure outlined below. The first 28 days of curing were the same for all specimens: immediately after casting, they were cured at T = 20 $\pm$ 1 °C and RH $>$ 95 % for 7 days (2 days in the molds, covered with plastic film, followed by demolding and covering with plastic film to prevent CO_2 ingress for additional 5 days). Then, they were exposed to natural carbonation at 20 $\pm$ 1 °C and 50 $\pm$ 5 % RH for the remaining 21 days.

Specimens S1 were tested after 2, 7, 14, 21, and 28 days of curing, in order to measure the evolution of pH during the standard curing regime of mortars on a weekly basis. Then, the specimens were divided into two series: the S2 series was placed in a box with continuous air renewal to enable natural carbonation (CO_2 = 0.03 vol%) at 20 $\pm$ 1 °C and 68 % RH, maintained by a saturated solution of potassium iodide (KI). The S3 series was placed in a carbonation chamber (T = 20 $\pm$ 1 °C, RH = 60 $\pm$ 5 %, CO_2 = 3 $\pm$ 0.2 vol%). Both S2 and S3 series underwent pH measurements after 35, 42, 63, 91, and 138 days of exposure. The measurements performed on S2 and S3 specimens groups were spaced out more overtime than those performed on S1 since it is well known that the front of carbonation proceeds by a parabolic law. The testing schedule is summarized in Table 1.

Table 1
Time test schedule of pH measurements on powders.

Curing period (days)	Curing conditions	pH measurements (days from the cast)		
		S1	S2 Natural CO_2 = 0.03 vol% RH = 68 %	S3 Accelerated CO_2 = 3 $\pm$ 0.2 vol% RH = 60 $\pm$ 5 %
From 0–7 (7 days)	T = 20 $\pm$ 1 °C RH $>$ 95 % CO_2 = none	2 7		
From 7–28 (21 days)	T = 20 $\pm$ 1 °C RH = 50 $\pm$ 5 % Natural CO_2 = 0.03 vol %	14 21 28		
From 28–138 (110 days)	T = 20 $\pm$ 1 °C		35 42 63 91 138	35 42 63 91 138

The paste alkalinity was also measured by the phenolphthalein test on unreinforced cubic specimens (100 mm per side), exposed to the same conditions as the cylindrical ones (see section 2.3.3) at specific time intervals. At each interval, the specimens were broken, and the internal surface was treated with a 1 % phenolphthalein solution in alcohol. In the uncarbonated portions of the specimen, where the mortar remains alkaline (pH $>$ 9), a purple-red coloration can be observed, while no surface color change occurs in the carbonated portions.

2.2.3. Corrosion behavior of rebars: electrochemical tests

For each mix, reinforcements corrosion was evaluated by electrochemical tests on one cylindrical specimen reinforced with two carbon steel (Fe) and two galvanized steel (Zn) corrugated rebars (Ø = 8 mm). The full scheme of cylindrical specimens dimensions, rebars length and positioning is reported in a previous paper [27]. Before the tests, carbon steel rebars were ground in order to remove possible corrosion products and cleaned with acetone to remove eventual grease on their surface. On the other hand, galvanized steel rebars were degreased with acetone and just before their embedment in the fresh mortars they were submerged for 5 s in 15 % NaOH solution to dissolve the $ZnCO_3$ layer eventually formed during atmospheric storage. The procedure of rebars preparation and reinforced cylindrical specimens casting is displayed in Fig. 1. After casting, the reinforced specimens were cured at RH $>$ 95 % and T = 20 $\pm$ 1 °C for the first 2 days and then at RH = 50 $\pm$ 5 % and T = 20 $\pm$ 1 °C. After 28 days of curing, the specimens were placed in an accelerated carbonation chamber (T = 21 $\pm$ 1 °C, RH = 60 $\pm$ 5 %, CO_2 = 3 $\pm$ 0.2 vol%) with the upper and lower surfaces of cylinders sealed by a two-component epoxy resin to ensure CO_2 penetration only through the lateral surface. The CO_2 concentration chosen in the present experimentation is in line with previous studies performed on carbonation of alkali-activated materials [46,47]. After that the carbonation of the 15 mm mortar cover was achieved, as detected by phenolphthalein test, the specimens were subjected to 12 weekly wet/dry cycles (1 day wet and 6 days dry) in tap water. The water used is potable water free from sediments, rust, heavy metals and contains negligible amounts of chlorides, which account to 24.1 mg/L; therefore, it is believed to have negligible effects on the test results.

The corrosion behavior was evaluated during both the accelerated carbonation, by free corrosion potential (E_{corr}) measurements, and the 12 weekly wet/dry cycles by E_{corr} and polarization resistance (R_p) measurements in wet conditions immediately before the specimens removal from the solution (Fig. 1). Free corrosion potential was

Fig. 1. Reinforced cylindrical specimens preparation: a. coated rebars, b. cylindrical molds, c. cylindrical mold with cover, d. corrosion measurements on specimens inside the molds, e. corrosion measurements on specimens outside the molds, f. corrosion measurements on specimens during wet/dry cycles in tap water (in the picture, measurements in wet condition are shown).

measured with a Saturated Calomel Electrode (SCE, +0.241 V vs SHE) as reference. The polarization resistance was determined by using an Amel workstation (566 function generator; 549 potentiostat; 621 differential electrometer) managed by a software suitably developed for using the Acquisition Board NI AT-MIO-16 (12 bit, 100k sample/s), adopting the galvanodynamic polarization method (scan rate = 0.5 μA/s; ΔV = ±5 mV) and calculating the average slopes of both the anodic and cathodic branches [27]. The electrochemical measurements (E_{corr} and R_p) were performed on the two rebars of the same type (bare and galvanized steels, respectively) immersed in each reinforced measurement; therefore, the reported results are the average value measured on each pair of rebars.

2.2.4. Corrosion behavior of rebars: visual and metallographic analysis

After the 12 weekly wet/dry cycles in tap water, to validate the corrosion data obtained by electrochemical tests, the cylindrical specimens were broken to allow the visual inspection of reinforcements and mortar at the rebar/mortar interface. Additionally, metallographic analysis was performed on the galvanized steel rebars. Small samples were embedded in a thermosetting resin and cross-sections polished firstly with emery paper up to 1200 grit and then with diamond powder down to 3 μm. Finally, the samples were etched in Nital 2 solution (2 vol % concentrated HNO_3 in ethanol) for 5 s, and the zinc coating thickness measured with an Olympus BX51 optical microscope. For each rebar, 60 measurements were taken, and the average values along with standard deviations reported.

3. Results and discussion

3.1. Mechanical and microstructural analyses of mortars

The compressive strength (R_c) of mortars after 28 days of curing is reported in Table 2. Both for CEM and AAMs, the required compressive

Table 2
Compressive strength (R_c) and total porosity (V_p) of cement-based and alkali-activated mortars after 28 days of curing.

Mixtures	R_c (MPa)	V_p (%)
R1 CEM	10.0 ± 0.3	25
R2 CEM	22.9 ± 0.7	24
R3 CEM	44.4 ± 3.6	18
R1 FANa	13.0 ± 0.9	19
R2 FANa	16.5 ± 1.8	16
R3 FANa	27.2 ± 2.4	15
R1 FAK	10.9 ± 0.7	17
R2 FAK	16.9 ± 1.8	14
R3 FAK	36.4 ± 1.0	13
R1 MKK	10.0 ± 2.0	35
R2 MKK	16.5 ± 1.0	35
R3 MKK	29.4 ± 3.9	34

strengths to satisfy the three different strength classes (i.e., R1 with $R_c \geq$ 10 MPa, R2 with $R_c \geq$ 15 MPa, and R3 with $R_c \geq$ 25 MPa, according to UNI EN 1504–3) have been reached.

The total porosity (V_p) of the mortars obtained by mercury intrusion porosimetry after 28 days of curing (Table 2) shows a decreasing trend, moving from R1 to R2 and R3 strength classes, as expected. The highest values are found for MKK mortars (around 35 %), followed by CEM mortars (between 25 % and 18 %), FANa mortars (between 19 % and 15 %), and finally by FAK ones (between 17 % and 13 %). In CEM mortars, this is related to the lower w/c ratio which gives a denser hydrated structure at a certain curing time. In AAMs, this is related both to the higher concentration of the activating solution and the lower water/binder ratio, which contribute to the greater densification of the paste [48]. The pore size distribution of mortars has been already reported in [27]. Following the classification of Kumar and Bhattacharjee [49], the microstructure of MKK and CEM mortars is characterized by capillary pores (10 nm $\leq$ d $\leq$ 1000 nm), which are smaller in the former compared to the latter, ranging from 70 to 30 nm and 100–50 nm, respectively. Conversely, FANa and FAK mortars have a more distributed porosity, with pores smaller than 15 and 30 nm if prepared with KOH and NaOH, respectively, and larger than 1 μm in both cases.

3.2. Alkalinity of paste during curing

The pH measurements performed throughout the curing period under natural carbonation are reported in Fig. 2. At the beginning of the test, AAMs are more alkaline than CEM due to the strong alkaline solutions used for their preparation. Indeed, during the first week of curing, both FANa and FAK mortars show a pH > 13.7 and MKK mortars a pH > 13.4, whereas CEM mortars register a pH around 13.2. Among AAMs, MKK mortars show the lowest pH because prepared with a less alkaline activating solution [41]. During the first weeks of curing, CEM mortars maintain their pH at about 13. On the contrary, AAMs undergo an alkalinity decrease due to the polymerization reaction which consumes the alkaline reagents to give neutral products. Nevertheless, FANa and FAK mortars show pH values higher than 13.4 after 28 days of curing, whereas a much high reduction of pH is found for MKK matrices. The alkalinity decrease of MKK mortars is the most pronounced due to their intrinsic polymerization reaction: as reported by Pouhet and Cyr [50], initially the OH^- provided by the activators results in a very high pH (around 14) but then some OH^- binds within the alkali-activated matrix, causing a rapid pH decrease until reaching a stationary condition. As a matter of fact, moving from R1 to R3 classes, the pH of MKK matrix ranges between 12.4 and 12.8 after 7 days and reaches values between 11.7 and 12.2 after 28 days of curing. Moreover, the higher porosity of MKK mortars with respect to CEM, FANa, and FAK ones (Table 2) facilitates the carbonation of pores solution which lowers the pH [50]. As expected, within the same mortar type, the alkalinity increases with the strength class owing to the lower w/c ratio for CEM mortars and the higher alkalinity of the activating solution for AAMs.

3.3. Alkalinity of paste during exposure to CO_2

After the first month of curing, both unreinforced cubic specimens and reinforced cylindrical specimens were inserted in the accelerated carbonation chamber. Some specimens of the same CEM and alkali-activated mortars were exposed to natural carbonation as reference for comparison.

In Fig. 3, the variation of paste pH both in atmospheric and $CO_2 = 3 \pm 0.2$ vol% rich environment is reported. In natural carbonation, the pH variations between 0.5–1.5 cm, 1.5–2.5 cm, and 2.5–3.5 cm are very limited. FANa and FAK mortars maintain the highest pH values (between 13 and 14) in all depths and for the entire test. On the other hand, in CEM mortars pH is stable at about 13 and in MKK mortars pH ranges from 12.5 to 11.5. Literature reports that under natural carbonation the reduction of pH below 10 appears unlikely in AAMs since the pore solution is usually dominated by sodium ions and the carbonate/bicarbonate equilibrium buffers the pH [3], as already explained in the introduction section. On the contrary, as expected, specimens exposed to accelerated carbonation exhibit elevated decrease of pH values, especially in the external depths and for the lower strength classes. The fastest decrease in paste alkalinity is found in CEM and MKK mortars, whereas for the less porous (Table 2) and highly alkaline FA-based mortars, the pH decrease is appreciable only at the most external depths of R1 strength class. Even if MKK mortars are more porous than CEM mortars (Table 2) and, at the end of curing, their pH is lower than that of CEM mortars (Fig. 2), the higher pH of MKK mortars with respect to CEM mortars measured on powders under accelerated carbonation could be due to the alkaline hydrolysis of Na_2CO_3 and K_2CO_3 formed by carbonation of AAMs matrices.

The phenolphthalein test (Fig. 4) provides a clear boundary between the carbonated and the uncarbonated regions only for CEM mortars. Indeed, only in this type of binder the pH reaches values lower than 9, that is the pH of phenolphthalein change from purple-red color to colorless. During accelerated carbonation, in AAMs mortars a pale pink color, even if lighter than in the central area, always appeared in the peripherical area of the section, more evident in MKK than in FANa and FAK mortars due to the lighter color (white) of the paste. This confirms that in AAMs the pH values are always higher than 9, also after 110 days of exposure to accelerated carbonation (Fig. 4), in agreement with pH measurements on powders (Fig. 3). For this reason, it was not possible to measure with certainty the carbonation depth of the studied AAMs, and therefore, these data are not given in the present paper. The difficulty of using phenolphthalein has been reported also in the literature [33] and related to the fact that the carbonated pore solution of AAMs has a pH within the color-change transition of the indicator. Therefore, the observation of any color change boundary may become arduous to detect visually or may emerge as a partially carbonated faint-pink zone. This effect can lead to complexities in carbonation depth measurements, causing systematic bias in readings performed on AAMs.

To evaluate if the carbonation rate is linked to the total porosity of mortars, given the impossibility of measuring carbonation depth, the

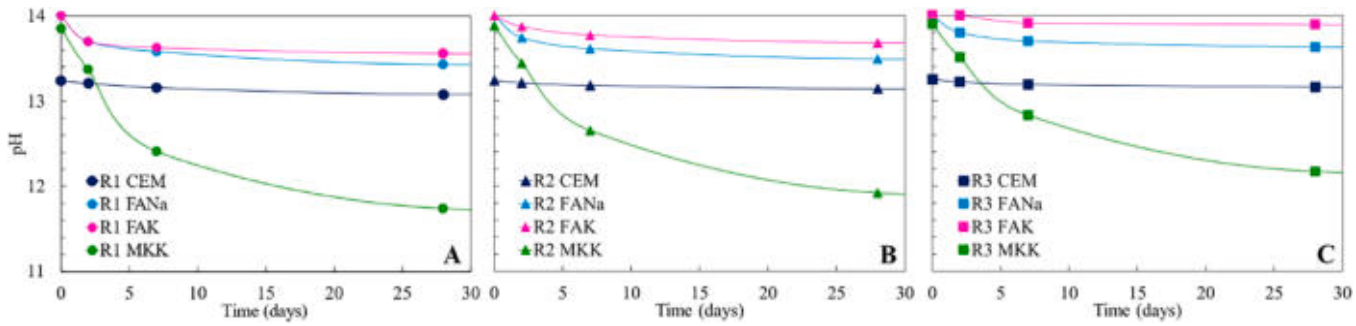

Fig. 2. pH measurements of mortars during the curing period belonging to R1 (A), R2 (B), R3 (C) strength classes.

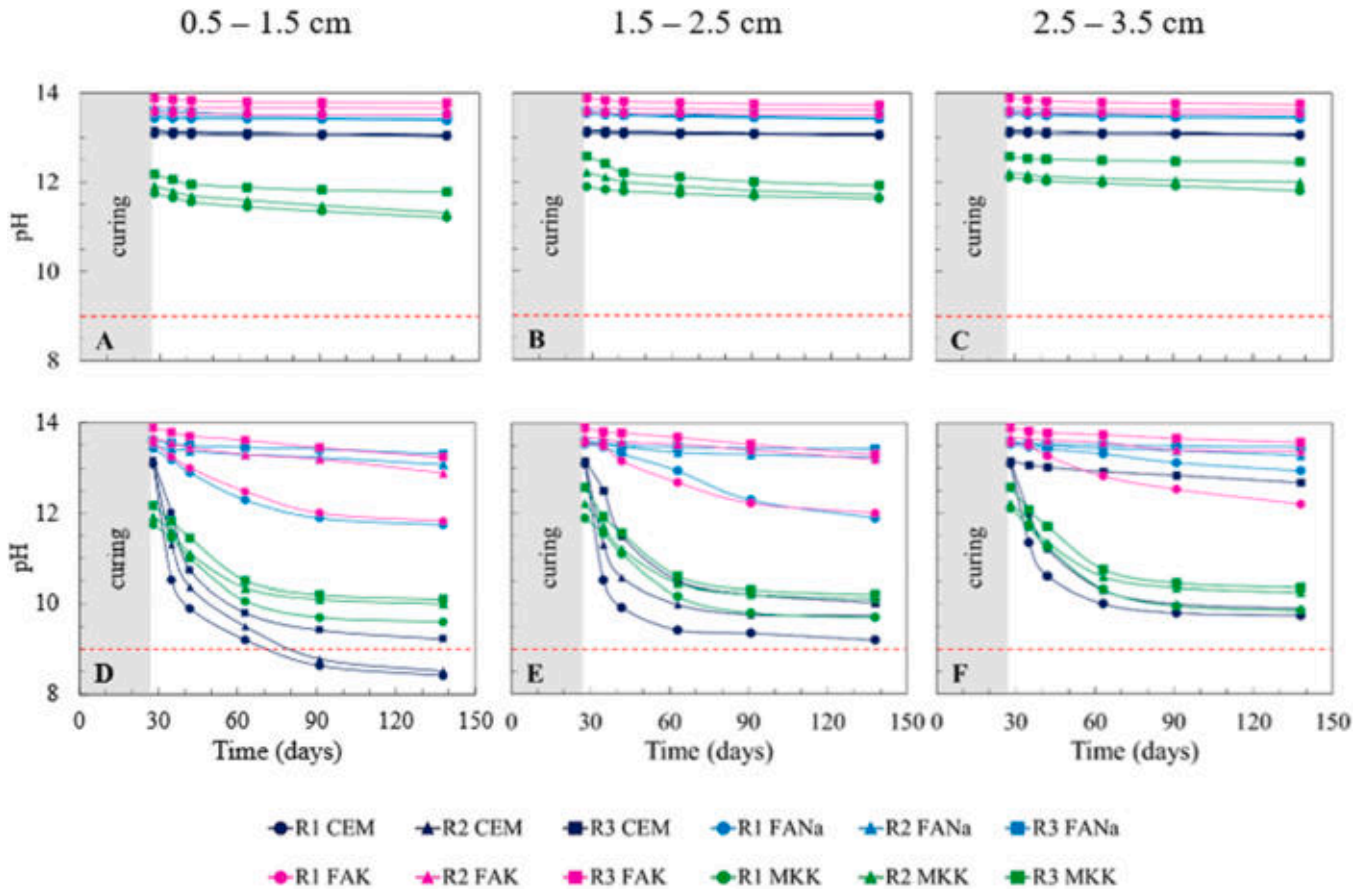

Fig. 3. pH measurements on powders of CEM and AA mortars exposed to natural (CO_2 = 0.03 vol%, A, B and C) and accelerated carbonation ($CO_2 = 3 \pm 0.2$ vol%, D, E and F) measured at the three different depths (0.5–1.5 cm, 1.5–2.5 cm, 2.5–3.5 cm). Red dashed line represents the pH = 9 threshold limit for steel rebars depassivation.

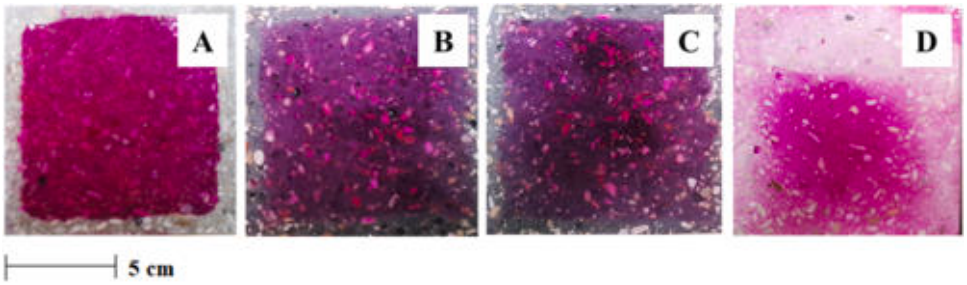

Fig. 4. Carbonation depth evaluated by phenolphthalein test of mortars exposed to accelerated carbonation ($CO_2 = 3 \pm 0.2$ vol%) for 70 days: A – R3 CEM, B – R3 FANa, C – R3 FAK, D – R3 MKK.

variation of pH (ΔpH) during accelerated carbonation in the most external depth (between 0.5 and 1.5 cm) and total porosity of mortars was studied (Fig. 5). As porosity increases, the pH variation also increases, except for MKK mortars. The greatest pH variation occurs in CEM mortars, since the formation of $CaCO_3$ reduces the alkalinity of the pore solution. Conversely, in AAMs the pH decreases less at the same V_p value, since the alkaline hydrolysis of carbonates partially restores the pH loss. Regarding MKK mortars, no correlation is found. Probably at a certain porosity, even if high, the buffering effect that restores the pH prevails on CO_2 ingress and therefore on carbonates formation. Indeed, the alkaline hydrolysis of Na_2CO_3 and K_2CO_3 does not significantly lower the pH. Furthermore, due to their high porosity, MKK mortars have already been significantly carbonated during the curing period (Fig. 2). For all these reasons, there is no correlation between total porosity and pH variation during accelerated carbonation for metakaolin-based mortars.

3.4. Corrosion behavior of rebars during exposure to CO_2: electrochemical tests

After approximately one week of exposure to accelerated carbonation, the E_{corr} values of bare steel rebars embedded in non-structural R1 and R2 CEM mortars significantly decrease from around 0 mV/SCE to −400 mV/SCE and −200 mV/SCE, respectively. These values continue to decline over the following week, reaching −500 mV/SCE for R1 CEM and −300 mV/SCE for R2 CEM (Figs. 6A and 6B). This reduction in E_{corr} values indicates an increased probability of corrosion: following ASTM C876 indications, a high probability of corrosion exists for bare steel when E_{corr} falls below −275 mV/SCE. The rapid carbonation of the cement paste, as corroborated by the swift decrease in pH to below 9

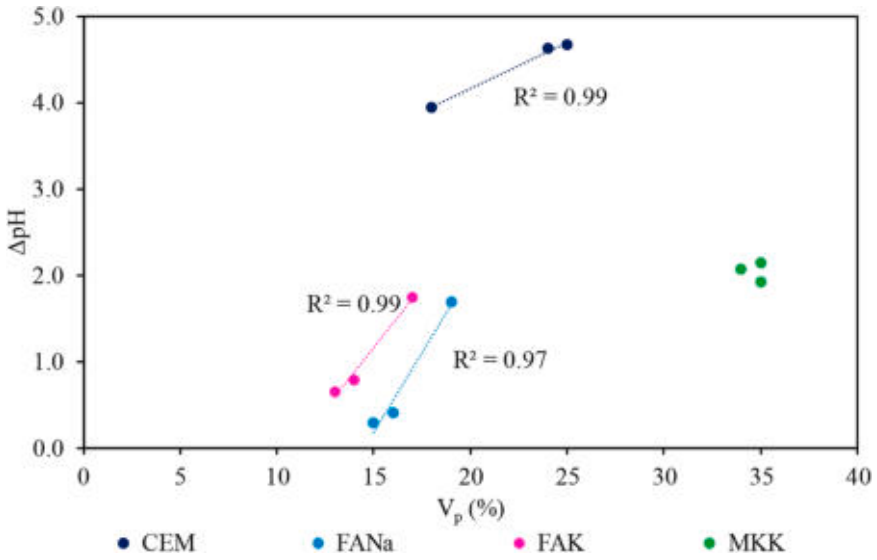

Fig. 5. Correlation between total porosity (V_p) and pH variation (ΔpH) of mortars during accelerated carbonation (from 28 to 138 days) measured on the 0.5–1.5 cm depth.

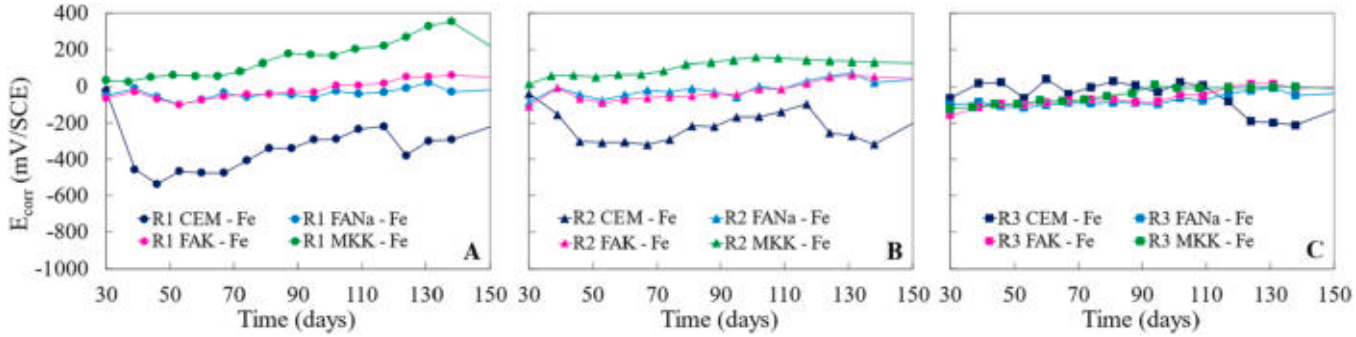

Fig. 6. Corrosion potential (E_{corr}) of steel rebars in CEM and AAMs mortars during the exposure to accelerated carbonation.

(Fig. 3), generally considered the upper threshold pH value for bare steel depassivation [4], compromises the passivation layer of bare steel, leaving it vulnerable to general corrosion. In R3 CEM mortar (Fig. 6C), E_{corr} values of bare steel remain higher for longer than in R2 and R1 CEM mortars and decrease gradually to around −200 mV/SCE, not reaching the −275 mV/SCE threshold E_{corr} values for rebar depassivation, meaning a low probability of corrosion. The final pH of 9.2 in R3 CEM mortar (Fig. 3), above the depassivation threshold of pH = 9, aligns with the observed lower probability of corrosion in this mortar. This higher pH value supports the maintenance of the passive layer on the rebar surface, helping to prevent corrosion initiation. Conversely, in R1, R2, and R3 AAMs, bare steel rebars appear unaffected by the CO_2-rich environment, with E_{corr} values stable at passive levels around 0 mV/SCE in FANa and FAK mortars and even slightly increasing in MKK mortars (Figs. 6A and 6B). This trend corresponds with the higher alkalinity compared to that of CEM mortars observed in Fig. 3: in FANa and FAK mortars, pH remains above 11 during accelerated carbonation, while in MKK mortar pH reduces to approximately 10, as also noted by Babaee [33]. All these pH values exceed the critical threshold of 9 for steel depassivation [4]. Therefore, for bare steel rebars, the accelerated carbonation gives a high probability of corrosion only in R1 and R2 CEM mortars (Fig. 6), while AAM mortars exhibit sufficient alkalinity to prevent steel depassivation and maintain corrosion resistance. As reported by Fernández-Jiménez et al. [51], the maintenance of alkalinity in the aqueous phase ensures steel to remain perfectly passive and immune to corrosion. Conversely, the reduction of alkalinity in the pore solution destroys the passive film of reinforcements, as occurred in the present study for bare steel embedded in R1 and R2 CEM mortars. The passive film of carbon steel has a double-layer structure: the inner contains mostly Fe^{II} oxides/oxyhydroxides and acts as barrier to aggressive elements while the outer mostly contains Fe^{III} oxides/oxyhydroxides. Fe^{III} layer being loose and porous does not play a positive role in passivation [52,53]. Therefore, the main contribution to the stability of the passive film is provided by Fe^{II} species; hence, the higher the content of Fe^{II} species, the higher the stability of the passive film [14]. When the pH of the pore solution decreases, the passive film becomes fragile and easily damageable by oxygen and various ions, thereby reducing its ability to protect the steel from corrosion.

For galvanized steel rebars, in R1 and R2 non-structural CEM mortars (Figs. 7A and 7B) the measured E_{corr} values decrease after the first week of exposure to accelerated carbonation and particularly in R1 CEM corrosion potential drops close to −1043 mV/SCE, which is generally considered the threshold E_{corr} value for galvanized steel depassivation [54], meaning a high probability of corrosion. In contrast, E_{corr} values for galvanized steel in R1 and R2 non-structural AAMs remain between −100 and −300 mV/SCE throughout the exposure period, indicating a low corrosion probability. In R3 structural mortars, E_{corr} values remain around −200 mV/SCE in CEM and fly ash-based AAMs, and at −400 mV/SCE in MKK mortars (Fig. 7C). Nonetheless, these values are still above the depassivation threshold, indicating a low probability of corrosion even under accelerated carbonation. Therefore, from these results, not only bare steel but also galvanized steel seem to have a high

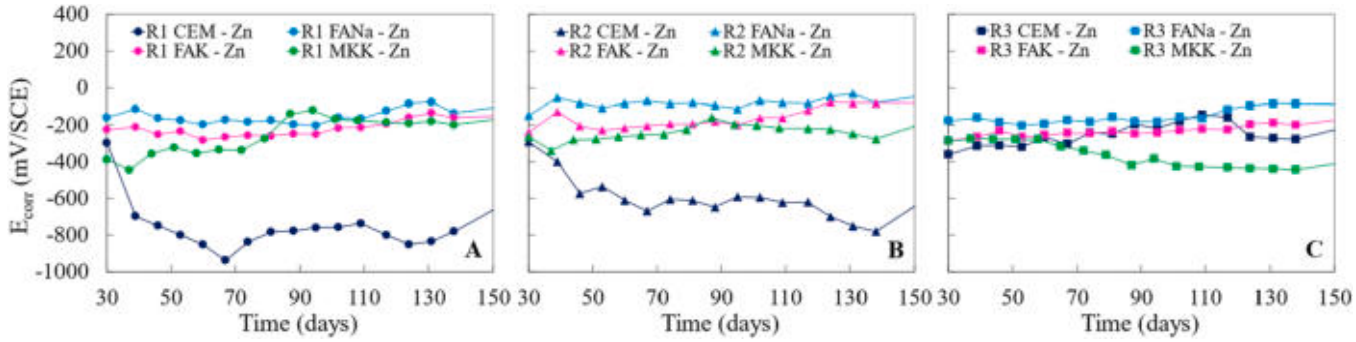

Fig. 7. Corrosion potential (E_{corr}) of galvanized steel rebars in CEM and AAMs mortars during the exposure to accelerated carbonation.

probability of corrosion only in R1 and R2 CEM mortars under accelerated carbonation conditions.

3.5. *Corrosion behavior of rebars during wet/dry cycles after carbonation: electrochemical tests*

After full carbonation of the mortar cover, all reinforced specimens underwent cyclic wet/dry exposure in tap water. In all CEM mortars, E_{corr} of bare steel drops to approximately −500 mV/SCE, regardless of the mortar strength class (Figs. 8A, 8B, 8C). In contrast, in AAMs bare steel maintains E_{corr} around 0 mV/SCE in all strength classes, indicating stability of the passive state. These E_{corr} findings align with the polarization resistance trends: immediately after the first water immersion, in CEM mortars R_p of bare steel falls below 10 kΩ•cm² (Figs. 7D, 7E, 7F), with a decline in R_p values from R3 to R1 CEM mortars, due to the increasing porosity of non-structural classes compared to the structural one (Table 2). Also MKK mortars exhibit R_p values below 10 kΩ•cm², though the correlation with the strength class is less clear likely due to the high porosity (~35 %) of MKK mortars, regardless of the strength class. Conversely, in FA-based mortars the R_p values remain constant and higher, at about 20 kΩ•cm² (Figs. 8D, 8E, 8F), for all the studied strength classes, consistent with their lower porosity and higher alkalinity compared to CEM and MKK mortars, which offer a less corrosive environment for bare steel. Thus, bare steel in CEM and MKK mortars, especially in lower strength classes, is more prone to corrosion than in FA-based mortars due to the combined effect of higher porosity and reduced alkalinity, which contribute to a more depassivating environment and promote steel corrosion [4].

After the initial immersion in tap water, in both CEM and MKK mortars, E_{corr} values of galvanized steel rebars quickly decrease around −1000 and −900 mV/SCE (Figs. 9A, 9B, 9C), due to the high porosity of these matrices. On the other hand, in FANa and FAK mortars E_{corr} values of galvanized steel maintain stable, except for a decrease to −400 mV/SCE in R3 FAK mortar (Fig. 9C), as reported in [27]. Polarization resistance measurements show that galvanized steel has a higher corrosion rate in non-structural R1 and R2 CEM mortars compared to AAMs. After immersion, R_p immediately drops to values as low as 5 kΩ•cm² in R1 CEM, progressively increasing across strength classes to 10 and 20 kΩ•cm² in R2 and R3 CEM, respectively (Figs. 9D, 9E, 9F). The high calcium content in CEM mortars can encourage the formation of a crystalline and protective calcium hydroxyzincate $Ca[Zn(OH)_3]_2 \cdot 2\,H_2O$ (CHZ) passivating layer on galvanized steel [38]. However, in cement-based materials, carbonation transforms the $Ca(OH)_2$ dissolved in the pore solution into $CaCO_3$ which then precipitates, decreases the pH, and converts CHZ to hydrozincite $Zn_5(CO_3)_2(OH)_6$ (HZ) [55], which is amorphous and less stable in water [18,56], according to the

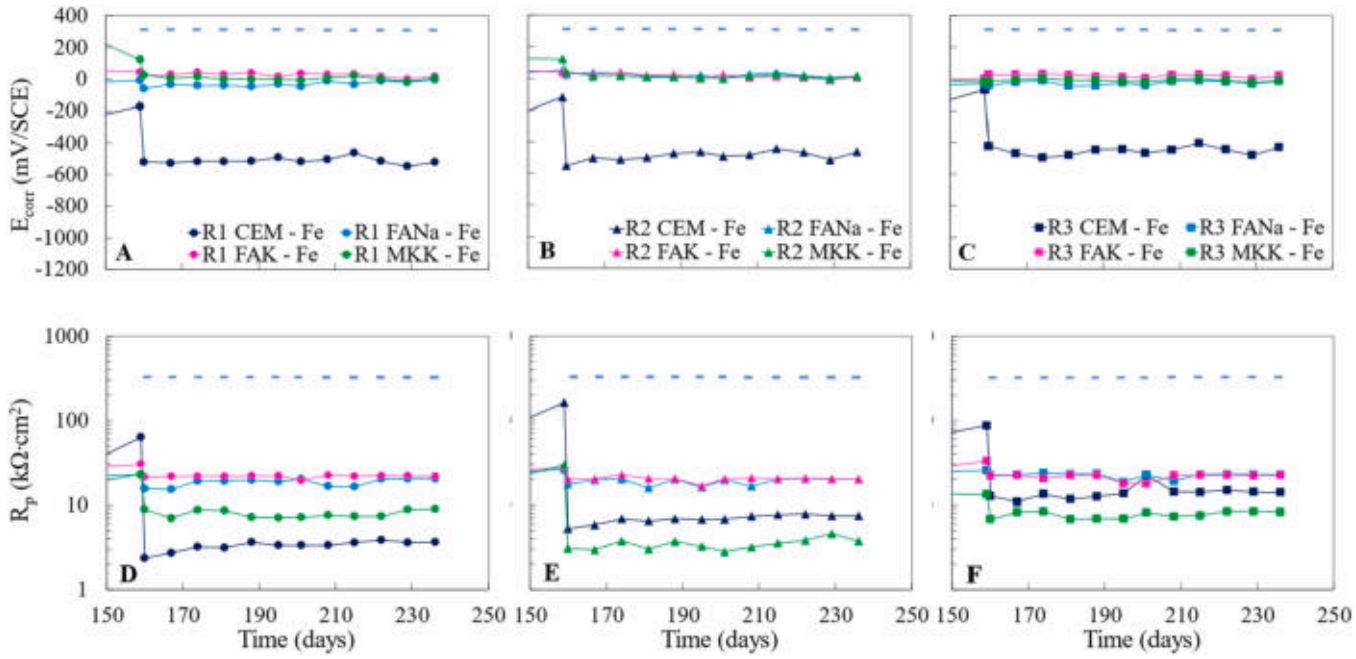

Fig. 8. Trends of corrosion potential (E_{corr}) and polarization resistance (R_p) of bare steel rebars embedded in CEM and AA mortars during wet/dry cycles in tap water belonging to R1 (A and D), R2 (B and E) and R3(C and F) strength classes. Blue lines represent wet condition periods.

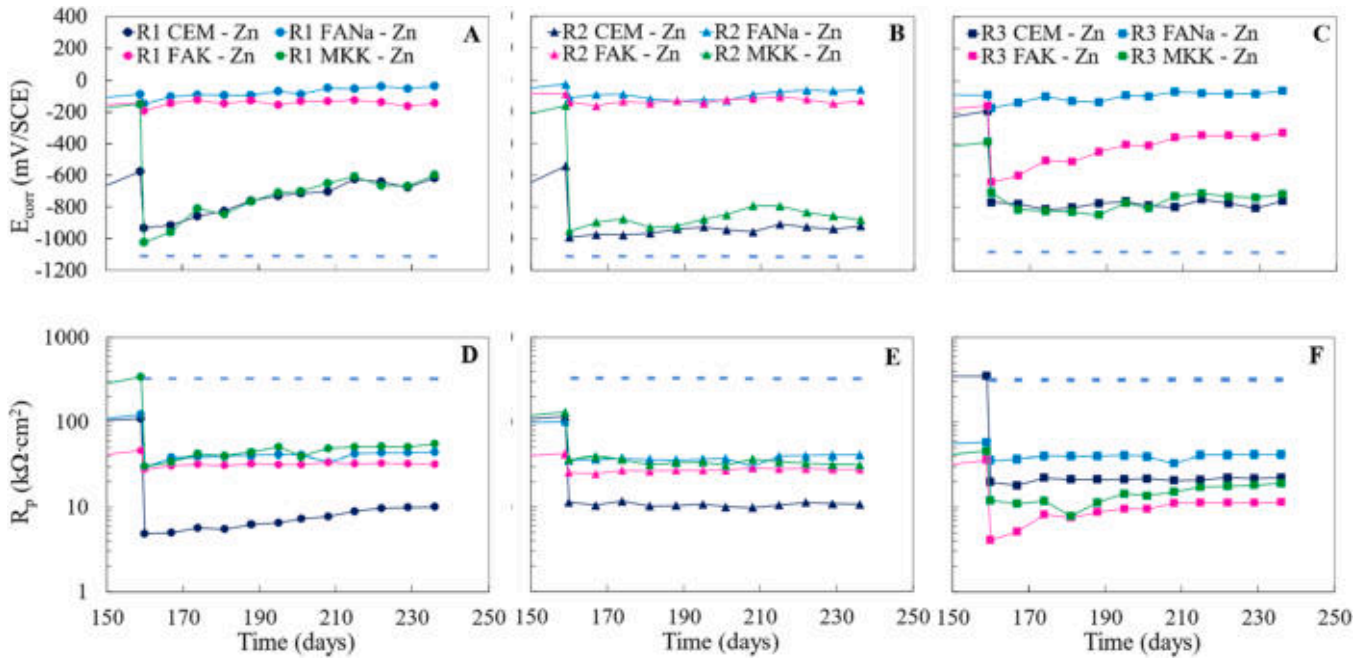

Fig. 9. Trends of corrosion potential (E_{corr}) and polarization resistance (R_p) of galvanized steel rebars embedded in CEM and AAMs during wet/dry cycles in tap water belonging to R1 (A and D), R2 (B and E) and R3 (C and F) strength classes. Blue lines represent wet condition periods.

following reaction:

$$5\ CaZn_2(OH)_6 \cdot 2H_2O + 9\ CO_2 \rightarrow 2\ Zn_5(CO_3)_2(OH)_6 + 5\ CaCO_3 + 19\ H_2O \quad (1)$$

This conversion, combined with the mortars high porosity, results in lower corrosion resistance of steel embedded in CEM mortars than in AAMs. Conversely, in AAMs the low calcium content precludes CHZ formation, as found also by other authors [57], but other passivating products may form, protecting the reinforcement from corrosion. Indeed, in alkaline environments the active zinc dissolution continues until the solution oversaturates by these ions, which then precipitate as ZnO or $Zn(OH)_2$ producing a continuous passivating layer [27]. On the other hand, CO_2 penetration can probably lead to the formation of $ZnCO_3$ or HZ, providing to galvanized steel protection against corrosion. In R1 and R2 AAMs the R_p of galvanized steel remains high and around 30–40 kΩ•cm² (Figs. 9D and 9E), while in R3 FAK mortar R_p declines to 10 kΩ•cm² (Fig. 9F). Considering R3 structural strength class, the highest corrosion rate is found for galvanized steel embedded in FAK mortars, as found by the authors in a previous study [27]. Indeed, after 28 days of curing, the high alkalinity of the paste consumes the η phase revealing zinc-iron alloys underneath [27]. These phases are less resistant to corrosion than the η one, due to the galvanic coupling between active zinc and passive iron. Therefore, the highest corrosion rate detected in R3 FAK mortars, could be due to two contributions: 1) the high alkalinity of the paste, which is aggressive for zinc-based products, and 2) the lower porosity of the matrix (Table 2), which precludes oxygen and CO_2 penetration. Therefore, also the formation of potentially passivating zinc corrosion products such as ZnO, $Zn(OH)_2$ and zinc hydroxycarbonates [55] is precluded being calcium absent. In R3 MKK mortar, the initial R_p values are lower than in R1 MKK and R2 MKK mortars likely due to the relatively higher alkalinity of the paste, as indicated in Fig. 3. However, during the subsequent wet/dry cycles, R_p increases to reach values similar to those measured in R3 CEM mortars. This gradual rise in R_p suggests that a passivation process is taking place, likely due to the formation of protective corrosion products on the reinforcement surface. These products inhibit corrosion by limiting the metal exposure to the electrolyte, thus enhancing the material overall corrosion resistance in this highly alkaline environment.

For the same type of mortar, a comparison of R_p values between bare and galvanized steel (Figs. 8 and 9) reveals that in cement-based mortars exposed to CO_2-rich environment bare steel is notably more susceptible to corrosion than galvanized steel, confirming the observations of Maahn and Sorensen [58]. Moreover, interestingly, this finding is not limited to CEM-based materials but also to AAMs.

3.6. *Corrosion behavior of rebars during wet/dry cycles after carbonation: autoptic evaluation and metallographic analysis*

Following the exposure to accelerated carbonation and the subsequent 12 weekly wet/dry cycles, to confirm the electrochemical results, autoptic and metallographic analyses were conducted on both bare and galvanized steel rebars extracted from reinforced specimens (Fig. 10). The findings reveal significant differences in corrosion of reinforcements embedded in different mortar types and strength classes.

Bare steel rebars display the most extensive corrosion in CEM mortars, with large areas covered by red rust, particularly in the two lower strength classes (R1 and R2). The visual evidence of red rust corresponds to the electrochemical results, which show low R_p values in CEM mortars (Fig. 8), particularly in R1 and R2, likely due to their high porosity (Table 2) and low alkalinity (Fig. 3). Steel in MKK mortars exhibits less severe corrosion than in CEM mortars but more than in FANa and FAK mortars, aligning with their intermediate electrochemical performance. Rebars embedded in FA-based mortars have minimal corrosion, with only small patches of red rust visible across all strength classes. These observations are consistent with the high measured R_p values (Fig. 8), which indicate greater resistance to corrosion due to the low porosity (Table 2) and high alkalinity (Fig. 3) of these matrices.

Galvanized steel reinforcements show a huge amount of white zinc corrosion products [27] in non-structural (R1 and R2) CEM mortars, which aligns with the low R_p values previously measured in these mortars (Fig. 9). In R3 CEM and in all R1, R2 and R3 FA-based mortars, white zinc corrosion products are minimal, suggesting high resistance to corrosion, in agreement again with the high R_p values measured in these matrices (Fig. 9). In MKK mortars, it is challenging to differentiate between white zinc corrosion products and the white adhered metakaolin paste. Additionally, a porous adhered paste is visible on galvanized steel

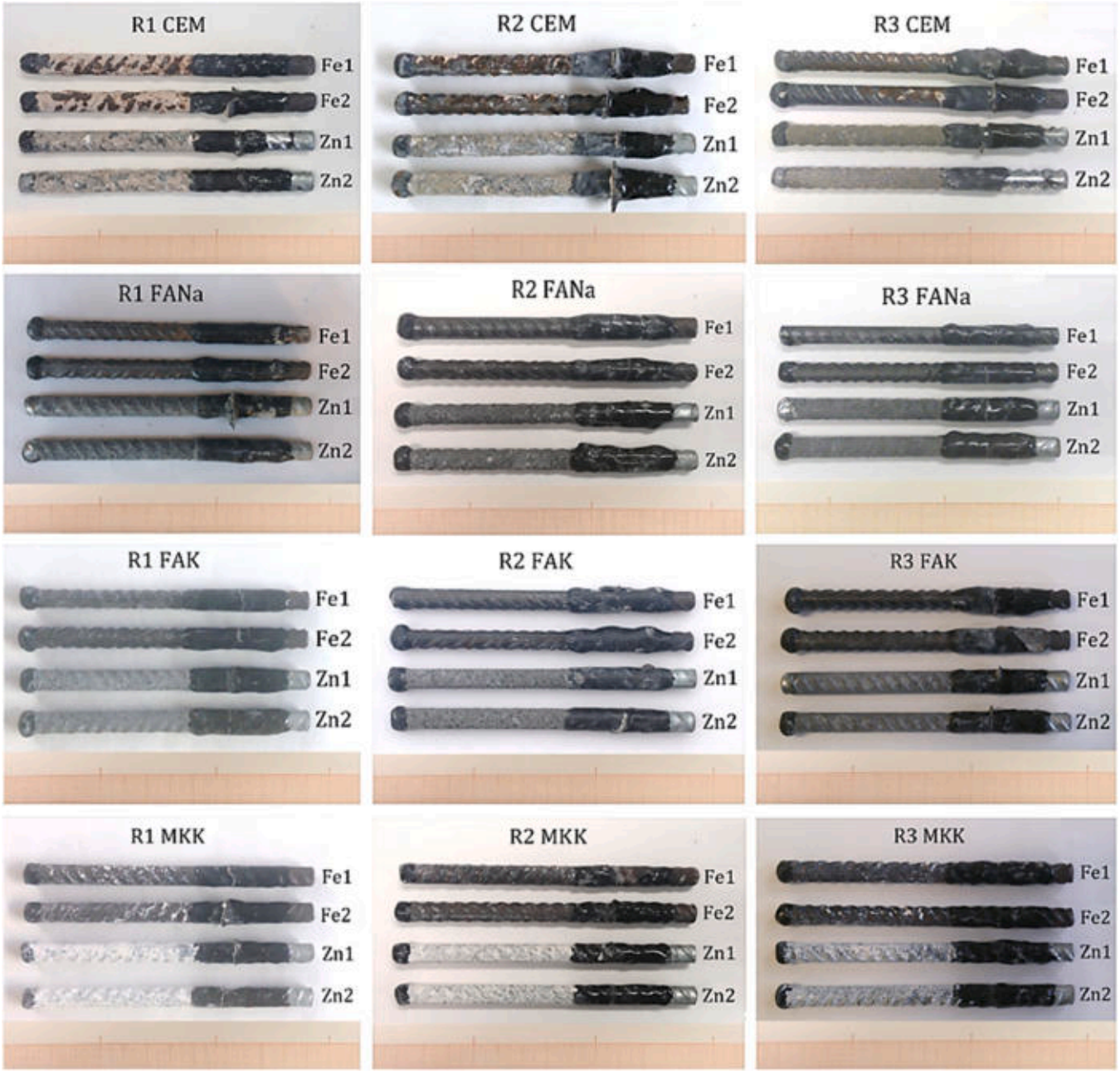

Fig. 10. Bare steel (Fe) and galvanized steel (Zn) rebars extracted from CEM and AA mortars after the exposure to wet/dry cycles in tap water.

rebars extracted from all AAMs (Fig. 11). This feature has been already noted by the authors [27] and attributed to the hydrogen formation at the mortar-reinforcement interface due to the reaction between the zinc coating and the extremely alkaline mortar matrix just after the casting.

Metallographic analysis of galvanized steel rebars extracted from the cylindrical specimens after the 12 wet/dry cycles, by measuring the reduction of the zinc coating (Fig. 12), reveals significant insights into the corrosion behavior across different mortars. For the sake of brevity, Fig. 13 provides detailed cross-sections for galvanized rebars embedded only in the R2 strength class mortars and the reference rebar not exposed to accelerated carbonation and wet/dry cycles in water (Fig. 13A). Non-structural CEM mortars (R1 and R2) have caused the highest reduction of the zinc coating thickness, of approximately 40 μm for R1 and 25 μm for R2. All other mortars give considerably better corrosion resistance to the embedded rebars, with a zinc layer reduction below 20 μm and the best protection offered by MKK mortars.

In R2 CEM mortar, the pure zinc layer (η phase) is fully corroded, exposing the iron-zinc alloys, demonstrating significant corrosion penetration (Fig. 13B), as expected by the low R_p measured in these matrices (Fig. 9). As previously reported (see Section 3.5), the high corrosion rate of galvanized steel embedded in CEM mortars (especially R1 and R2) can be attributed to their high porosity (Table 2) and to the conversion of CHZ in an instable passive film of HZ formed after carbonation [55], which offers limited protection during wet/dry cycles. In R2 FANa and R2 FAK mortars, although the pure zinc layer is consumed as in CEM, the zinc-iron alloys are present and only mildly affected (Figs. 13C and 13D). This suggests that, even if FA-based mortars retain some corrosion resistance, given also by the high R_p values generally measured (Fig. 9), the highly alkaline environment of the first days after casting (Fig. 2) is the main cause of the zinc consumption [27]. Since Zn-Fe alloys are more noble than pure Zn, this can justify the less negative E_{corr} measured in FA-based than in CEM-based

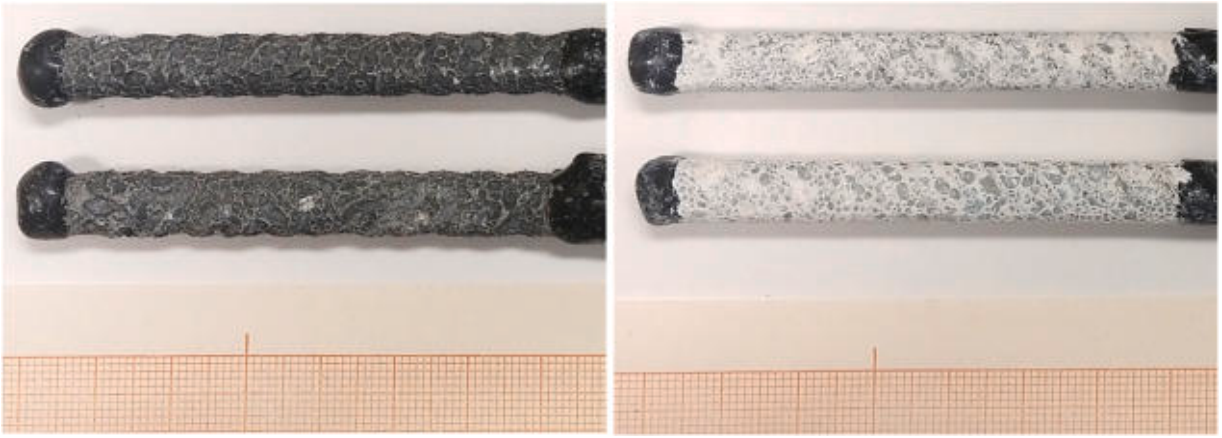

Fig. 11. Galvanized steel rebars extracted from R2 FAK (left) and R2 MKK (right) mortars after the exposure to wet/dry cycles in tap water. Magnification of the porous adhered paste on galvanized steel surface.

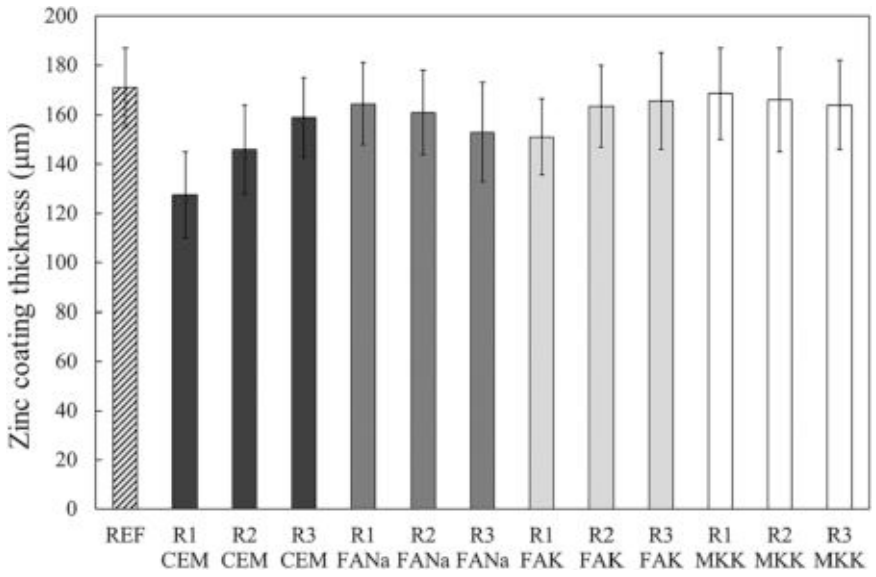

Fig. 12. Thickness of the remaining zinc coating on galvanized steel rebars embedded in CEM and AAMs after the exposure to wet/dry cycles in tap water evaluated by metallographic analysis. REF refers to the reference rebar not exposed to accelerated carbonation and wet/dry cycles in water.

matrices during exposure to accelerated carbonation (Fig. 7) and the following wet/dry cycles in water (Fig. 9) and the apparent discrepancy between the less negative E_{corr} but lowest R_p values measured in R3 FAK mortars (Fig. 9).

In R2 MKK mortar, the η phase is still visible on the rebar surface (Fig. 13E), confirming that MKK mortars provide the most favorable environment for galvanized steel protection. This superior performance in MKK mortars is likely due to the combination of two properties: low alkalinity (less aggressive toward zinc, see Figs. 2 and 3), and high porosity (Table 2), facilitating the penetration of oxygen and CO_2 which in turn promote the formation of a passivating layer of zinc corrosion products (e.g., ZnO, $Zn(OH)_2$, and $ZnCO_3$) [55] in the absence of calcium.

4. Conclusions

This study evaluated the corrosion behavior of bare and galvanized steel reinforcements embedded in various mortars, including cement (CEM) and alkali-activated materials (AAMs) derived from Class F fly ash (labelled as FANa and FAK) or metakaolin (labelled as MKK). Mortars of three strength classes (R1 with $R_c \geq 10$ MPa, R2 with $R_c \geq 15$ MPa, R3 with $R_c \geq 25$ MPa) were exposed to an accelerated carbonation environment (3 vol% CO_2) followed by 12 weekly wet/dry cycles in tap water. Electrochemical measurements, visual observations, and metallographic analysis assessed CO_2-induced corrosion, and the results were correlated with paste alkalinity in different binders during curing and CO_2 exposure.

Results have shown that after 28 days of curing fly ash-based AAMs display the highest pH; conversely, MKK ones exhibit the lowest pH due to their highest porosity and lowest alkalinity of the activating solution. Accelerated carbonation at 3 vol% CO_2 reduces the pH much more than natural carbonation in outermost areas of the material and it is much more aggressive for materials with high porosity. Indeed, fly ash-based AAMs are much less affected by pH reduction, thanks to their higher initial alkalinity and low porosity. Moreover, during accelerated carbonation the pH goes below 9 only in R1 and R2 CEM mortars, determining a high probability of corrosion on both bare and galvanized steel rebars. In any case, accelerated carbonation is much more aggressive for bare steel than for galvanized steel. Indeed, bare steel rebars show an initial active corrosion and continue to corrode in all mortars during wet/dry cycles in water, even though those embedded in fly ash AAMs seem to be the least affected.

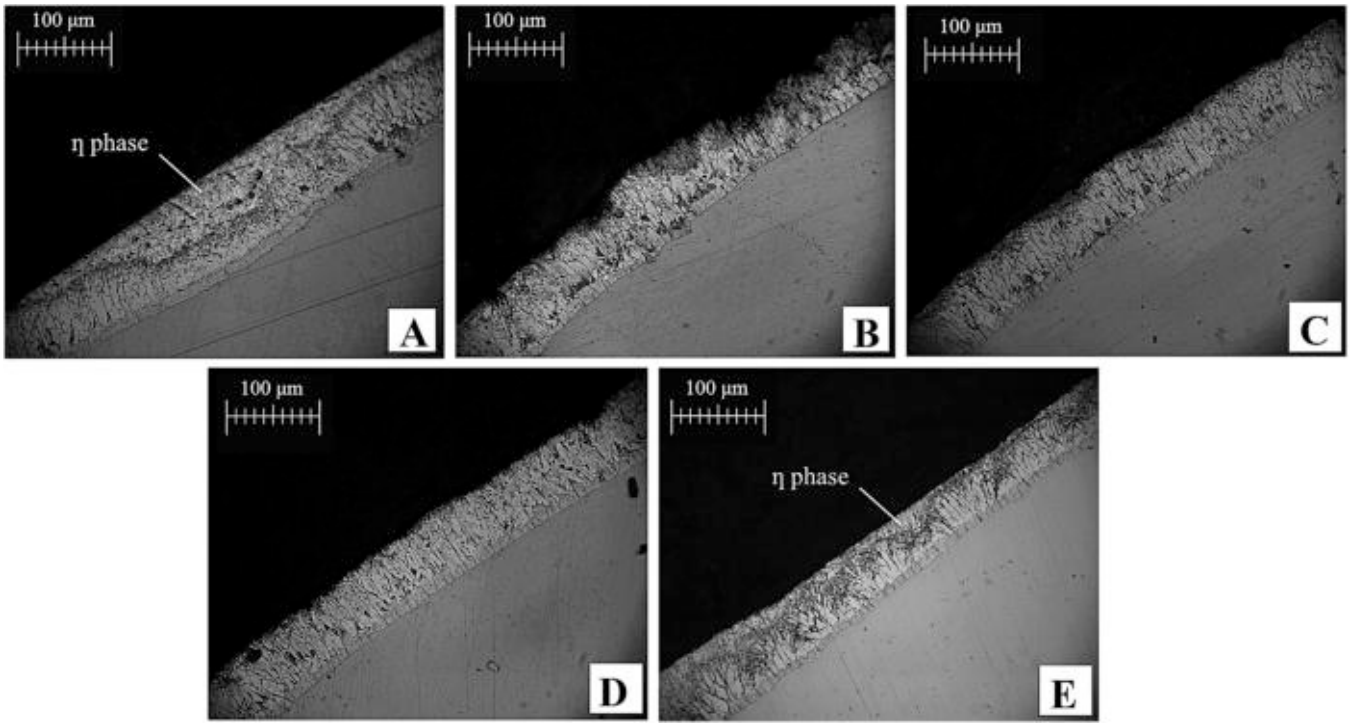

Fig. 13. Metallographic cross-section of galvanized steel rebars after the exposure to wet/dry cycles in tap water embedded in A. epoxy resin as reference, B. R2 CEM, C. R2 FANa, D. R2 FAK, E. R2 MKK.

Generally, AAMs and particularly those based on metakaolin, provide the lowest zinc coating consumption on galvanized steel, thanks to the optimal balance of low alkalinity and high porosity, which facilitates O_2 and CO_2 ingress, promoting potentially passivating zinc corrosion products (e.g., ZnO, $Zn(OH)_2$, and $ZnCO_3$). For this reason, the use of galvanized steel reinforcements and metakaolin-based alkali-activated materials can be an optimal choice for those structures prone to carbonation.

CRediT authorship contribution statement

Francesca Tittarelli: Writing – review & editing, Supervision, Resources, Funding acquisition, Conceptualization. **Chiara Giosuè:** Writing – review & editing, Validation, Software, Methodology, Investigation, Formal analysis, Data curation, Conceptualization. **MOBILI ALESSANDRA:** Writing – original draft, Validation, Software, Methodology, Investigation, Formal analysis, Data curation, Conceptualization. **Tiziano Bellezze:** Writing – review & editing, Supervision, Resources, Data curation, Conceptualization.

Declaration of Competing Interest

The authors declare that they have no known competing financial interests or personal relationships that could have appeared to influence the work reported in this paper.

Acknowledgements

The authors would like to thank Ingessil S.r.l. (Verona, Italy) for the sodium silicate solution and General Admixture S.p.A. (Ponzano Veneto, Italy) for the fly ash kindly offered for this study.

Data availability

Data will be made available on request.

References

[1] A. Belli, A. Mobili, T. Bellezze, F. Tittarelli, P.B. Cachim, Evaluating the self-sensing ability of cement mortars manufactured with graphene nanoplatelets, virgin or recycled carbon fibers through piezoresistivity tests, Sustainability 10 (2018) 4013, https://doi.org/10.3390/su10114013.
[2] C. Giosuè, A. Mobili, C. Di Perna, F. Tittarelli, Performance of lightweight cement-based and alkali-activated mortars exposed to high-temperature, Constr. Build. Mater. 220 (2019) 565–576, https://doi.org/10.1016/j.conbuildmat.2019.05.193.
[3] S.A. Bernal, J.L. Provis, D.G. Brice, A. Kilcullen, P. Duxson, J.S.J. Van Deventer, Accelerated carbonation testing of alkali-activated binders significantly underestimates service life: the role of pore solution chemistry, Cem. Concr. Res. 42 (2012) 1317–1326, https://doi.org/10.1016/j.cemconres.2012.07.002.
[4] M. Pourbaix, Atlas of electrochemical equilibria in aqueous solutions, National Association of Corrosion Engineers, Houston, Texas, USA, 1974.
[5] P. Duxson, J.L. Provis, G.C. Lukey, J.S.J. van Deventer, The role of inorganic polymer technology in the development of "green concrete,", Cem. Concr. Res. 37 (2007) 1590–1597, https://doi.org/10.1016/j.cemconres.2007.08.018.
[6] A. Mobili, A. Belli, C. Giosuè, A. Telesca, M. Marroccoli, F. Tittarelli, Calcium sulfoaluminate, geopolymeric, and cementitious mortars for structural applications, Environments 4 (2017) 64, https://doi.org/10.3390/environments4030064.
[7] A. Mobili, A. Telesca, M. Marroccoli, F. Tittarelli, Calcium sulfoaluminate and alkali-activated fly ash cements as alternative to Portland cement: study on chemical, physical-mechanical, and durability properties of mortars with the same strength class, Constr. Build. Mater. 246 (2020) 118436, https://doi.org/10.1016/j.conbuildmat.2020.118436.
[8] J.L. Provis, Alkali-activated materials, Cem. Concr. Compos 114 (2018) 40–48, https://doi.org/10.1016/j.cemconres.2017.02.009.
[9] J. Davidovits, Geopolymers: Inorganic polymeric new materials, J. Therm. Anal. 37 (1991) 1633–1634, https://doi.org/10.1007/BF01912193.
[10] O.A. Mohamed, A Review of durability and strength characteristics of alkali-activated slag concrete, Materials 12 (2019) 1198, https://doi.org/10.3390/ma12081198.
[11] D.E. Cadore, C. Angulski da Luz, M.H. Farias de Medeiros, An investigation of the carbonation of alkaline activated cement made from blast furnace slag generated by charcoal, Constr. Build. Mater. 226 (2019) 117–125, https://doi.org/10.1016/j.conbuildmat.2019.07.209.
[12] D.E. Angulo-Ramirez, R. Mejía de Gutiérrez, W.G. Valencia-Saavedra, M.H.F. de Medeiros, J. Hoppe-Filho, Carbonation of hybrid concrete with high blast furnace slag content and its impact on structural steel corrosion, Mater. ConstrucciónN. 69 (2019) 182, https://doi.org/10.3989/mc.2019.05418.
[13] B. Kraft, M. Müller, R. Achenbach, H.-M. Ludwig, M. Raupach, Carbonation behaviour of concretes with alternative binders at different CO2 concentrations, Ce/Pap. 6 (2023) 1334–1341, https://doi.org/10.1002/cepa.3000.

[14] X. Xu, X. Hu, A. Khaskhoussi, C. Shi, Passivation and depassivation of reinforcement steel in alkali-activated materials - A review, Cem. Concr. Compos 154 (2024) 105802, https://doi.org/10.1016/j.cemconcomp.2024.105802.
[15] M. Nedeljković, B. Ghiassi, S. Melzer, C. Kooij, S. van der Laan, G. Ye, CO2 binding capacity of alkali-activated fly ash and slag pastes, Ceram. Int. 44 (2018) 19646–19660, https://doi.org/10.1016/j.ceramint.2018.07.216.
[16] A.M. Rashad, A synopsis of carbonation of alkali-activated materials, Green. Mater. 7 (2019) 118–136, https://doi.org/10.1680/jgrma.18.00052.
[17] Z. Li, S. Li, Carbonation resistance of fly ash and blast furnace slag based geopolymer concrete, Constr. Build. Mater. 163 (2018) 668–680, https://doi.org/10.1016/j.conbuildmat.2017.12.127.
[18] A. Mobili, C. Giosuè, T. Bellezze, F. Tittarelli, Corrosion behavior of galvanized and bare steel reinforcements embedded in carbonated alkali-activated metakaolin mortar, Metall. Ital. (2020) 22–26.
[19] Z. Sun, A. Vollpracht, One year geopolymerisation of sodium silicate activated fly ash and metakaolin geopolymers, Cem. Concr. Compos 95 (2019) 98–110, https://doi.org/10.1016/j.cemconcomp.2018.10.014.
[20] M. Sufian Badar, K. Kupwade-Patil, S.A. Bernal, J.L. Provis, E.N. Allouche, Corrosion of steel bars induced by accelerated carbonation in low and high calcium fly ash geopolymer concretes, Constr. Build. Mater. 61 (2014) 79–89, https://doi.org/10.1016/j.conbuildmat.2014.03.015.
[21] V. Charitha, G. Athira, A. Bahurudeen, S. Shekhar, Carbonation of alkali activated binders and comparison with the performance of ordinary Portland cement and blended cement binders, J. Build. Eng. 53 (2022) 104513, https://doi.org/10.1016/j.jobe.2022.104513.
[22] H. Kim, K. Song, J. Song, J.G. Jang, Effect of carbonation on abrasion resistance of alkali-activated slag with various activators, Mater. (Basel) 12 (2019) 2812, https://doi.org/10.3390/ma12172812.
[23] M. Nedeljković, B. Šavija, Y. Zuo, M. Luković, G. Ye, Effect of natural carbonation on the pore structure and elastic modulus of the alkali-activated fly ash and slag pastes, Constr. Build. Mater. 161 (2018) 687–704, https://doi.org/10.1016/j.conbuildmat.2017.12.005.
[24] R. Navarro, E.G. Alcocel, I. Sánchez, P. Garcés, E. Zornoza, Corrosion resistance of steel reinforcements embedded in alkali activated ground granulated SiMn slag mortars, Constr. Build. Mater. 230 (2020) 116917, https://doi.org/10.1016/j.conbuildmat.2019.116917.
[25] J. Zhang, C. Shi, Z. Zhang, Carbonation induced phase evolution in alkali-activated slag/fly ash cements: The effect of silicate modulus of activators, Constr. Build. Mater. 223 (2019) 566–582, https://doi.org/10.1016/j.conbuildmat.2019.07.024.
[26] K. Pasupathy, M. Berndt, J.G. Sanjayan, P. Rajeev, D.S. Cheema, Durability performance of precast fly ash – based geopolymer concrete under atmospheric exposure conditions, J. Mater. Civ. Eng. 30 (2018) 04018007, https://doi.org/10.1061/(ASCE)MT.1943-5533.0002165.
[27] F. Tittarelli, A. Mobili, C. Giosuè, A. Belli, T. Bellezze, Corrosion behaviour of bare and galvanized steel in geopolymer and Ordinary Portland Cement based mortars with the same strength class exposed to chlorides, Corros. Sci. 134 (2018) 64–77, https://doi.org/10.1016/j.corsci.2018.02.014.
[28] Z. Tian, C. Fu, H. Ye, How does carbonation of alkali-activated slag and Portland cement systems impact steel corrosion differently? Cem. Concr. Res. 181 (2024) 107528 https://doi.org/10.1016/j.cemconres.2024.107528.
[29] T. Bakharev, J.G. Sanjayan, Y. Cheng, Resistance of alkali-activated slag concrete to carbonation, Cem. Concr. Res. 31 (2001) 1277–1283, https://doi.org/10.1016/S0008-8846(01)00574-9.
[30] J. Shi, Z. Geng, X. Zhou, Reinforcing steels in low-carbon mortars subjected to chloride attack and natural carbonation: contradictory trends in passivation ability and corrosion resistance, Cem. Concr. Compos 152 (2024) 105666, https://doi.org/10.1016/j.cemconcomp.2024.105666.
[31] X. Zhou, M. Li, J. Shi, Role of sodium citrate in electrochemical behavior of reinforcing steel exposed to carbonated alkali-activated fly ash contaminated with chloride ions, Constr. Build. Mater. 445 (2024) 137913, https://doi.org/10.1016/j.conbuildmat.2024.137913.
[32] K. Pasupathy, J. Sanjayan, P. Rajeev, Evaluation of alkalinity changes and carbonation of geopolymer concrete exposed to wetting and drying, J. Build. Eng. 35 (2021) 102029, https://doi.org/10.1016/j.jobe.2020.102029.
[33] M. Babaee, M.S.H. Khan, A. Castel, Passivity of embedded reinforcement in carbonated low-calcium fly ash-based geopolymer concrete, Cem. Concr. Compos 85 (2018) 32–43, https://doi.org/10.1016/j.cemconcomp.2017.10.001.
[34] Y.-H. Bai, Y. Sheng, C. Wei, Experimental study of carbonation resistance of alkali-activated slag concrete, Acids Mater. J. 116 (2019) 95–104.
[35] M. Nedeljkovi, B. Ghiassi, S. van der Laan, Z. Li, G. Ye, Effect of curing conditions on the pore solution and carbonation resistance of alkali-activated fly ash and slag pastes, Cem. Concr. Res. 116 (2019) 146–158, https://doi.org/10.1016/j.cemconres.2018.11.011.
[36] S. Liu, Y. Hao, G. Ma, Approaches to enhance the carbonation resistance of fly ash and slag based alkali-activated mortar- experimental evaluations, J. Clean. Prod. 280 (2021) 124321, https://doi.org/10.1016/j.jclepro.2020.124321.
[37] T. Bellezze, A. Mobili, F. Tittarelli, Durability benefits of galvanized steel in reinforced concrete under different exposure conditions, in: B. Belletti, D. Coronelli (Eds.), Work. Capacit. Assess. Corroded Reinf. Concr. Struct. Fib CACRCS DAYS, 2021, 2021, pp. 45–48.
[38] T. Bellezze, G. Roventi, E. Barbaresi, N. Ruffini, R. Fratesi, Effect of concrete carbonation process on the passivating products of galvanized steel reinforcements, Mater. Corros. 62 (2011) 155–160, https://doi.org/10.1002/maco.201005776.
[39] A. Mobili, A. Belli, C. Giosuè, T. Bellezze, F. Tittarelli, Corrosion behavior of galvanized steel reinforcements in geopolymeric and cementitious mortars at the same strength class | [Comportamento a corrosione di armature zincate in malte geopolimeriche e cementizie a parità di classe di resistenza], Metall. Ital. 109 (2017) 47–50.
[40] J. Zhang, C. Shi, Z. Zhang, Z. Ou, Durability of alkali-activated materials in aggressive environments: a review on recent studies, Constr. Build. Mater. 152 (2017) 598–613, https://doi.org/10.1016/j.conbuildmat.2017.07.027.
[41] A. Mobili, A. Belli, C. Giosuè, T. Bellezze, F. Tittarelli, Metakaolin and fly ash alkali-activated mortars compared with cementitious mortars at the same strength class, Cem. Concr. Res. 88 (2016) 198–210, https://doi.org/10.1016/j.cemconres.2016.07.004.
[42] S.A. Bernal, Effect of the activator dose on the compressive strength and accelerated carbonation resistance of alkali silicate-activated slag/metakaolin blended materials, Constr. Build. Mater. 98 (2015) 217–226, https://doi.org/10.1016/j.conbuildmat.2015.08.013.
[43] C. Monticelli, M.E. Natali, A. Balbo, C. Chiavari, F. Zanotto, S. Manzi, M. C. Bignozzi, A study on the corrosion of reinforcing bars in alkali-activated fly ash mortars under wet and dry exposures to chloride solutions, Cem. Concr. Res. 87 (2016) 53–63, https://doi.org/10.1016/j.cemconres.2016.05.010.
[44] C. Monticelli, M. Criado, S. Fajardo, J.M. Bastidas, M. Abbottoni, A. Balbo, Corrosion behaviour of a Low Ni austenitic stainless steel in carbonated chloride-polluted alkali-activated fly ash mortar, Cem. Concr. Res. 55 (2014) 49–58, https://doi.org/10.1016/j.cemconres.2013.09.014.
[45] V. Räsänen, V. Penttala, The pH measurement of concrete and smoothing mortar using a concrete powder suspension, Cem. Concr. Res. 34 (2004) 813–820, https://doi.org/10.1016/j.cemconres.2003.09.017.
[46] S.A. Bernal, R.M. De Gutiérrez, J.L. Provis, V. Rose, Effect of silicate modulus and metakaolin incorporation on the carbonation of alkali silicate-activated slags, Cem. Concr. Res. 40 (2010) 898–907, https://doi.org/10.1016/j.cemconres.2010.02.003.
[47] S.A. Bernal, J.L. Provis, B. Walkley, R. San Nicolas, J.D. Gehman, D.G. Brice, A. R. Kilcullen, P. Duxson, J.S.J. van Deventer, Gel nanostructure in alkali-activated binders based on slag and fly ash, and effects of accelerated carbonation, Cem. Concr. Res. 53 (2013) 127–144, https://doi.org/10.1016/j.cemconres.2013.06.007.
[48] P. Chindaprasirt, W. Chalee, Effect of sodium hydroxide concentration on chloride penetration and steel corrosion of fly ash-based geopolymer concrete under marine site, Constr. Build. Mater. 63 (2014) 303–310, https://doi.org/10.1016/j.conbuildmat.2014.04.010.
[49] R. Kumar, B. Bhattacharjee, Porosity, pore size distribution and in situ strength of concrete, Cem. Concr. Res. 33 (2003) 155–164, https://doi.org/10.1016/S0008-8846(02)00942-0.
[50] R. Pouhet, M. Cyr, Carbonation in the pore solution of metakaolin-based geopolymer, Cem. Concr. Res. 88 (2016) 227–235, https://doi.org/10.1016/j.cemconres.2016.05.008.
[51] A. Fernández-Jiménez, J.M. Miranda, J.A. González, A. Palomo, Steel passive state stability in activated fly ash mortars, Mater. ConstrucciÓN. 60 (2010) 51–65, https://doi.org/10.3989/mc.2010.53909.
[52] J. Williamson, O.B. Isgor, The effect of simulated concrete pore solution composition and chlorides on the electronic properties of passive films on carbon steel rebar, Eval. Program Plann 106 (2016) 82–95, https://doi.org/10.1016/j.corsci.2016.01.027.
[53] H. Ji, Y. Tian, R. Zhao, N. Jin, X. Jin, Z. Tian, D. Yan, Passivation and depassivation of hpb335 carbon steel in simulated concrete pore solution, Int. J. Electrochem. Sci. 15 (2020) 6488–6507, https://doi.org/10.20964/2020.07.43.
[54] F.A. Cedrim, V.L.S. Almeida, C.A.C. Souza, M.D. Jesus, D.V. Ribeiro, Effects of the zinc and zinc-nickel alloys electroplating on the corrodibility of reinforced concrete rebars, Rev. IBRACON Estrut. e Mater. 9 (2016) 595–605, https://doi.org/10.1590/S1983-41952016000400008.
[55] G. Roventi, T. Bellezze, E. Barbaresi, R. Fratesi, Effect of carbonation process on the passivating products of zinc in Ca(OH)2 saturated solution, Mater. Corros. 64 (2013) 1007–1014, https://doi.org/10.1002/maco.201206868.
[56] G. Roventi, T. Bellezze, G. Giuliani, C. Conti, Corrosion resistance of galvanized steel reinforcements in carbonated concrete: effect of wet-dry cycles in tap water and in chloride solution on the passivating layer, Cem. Concr. Res. 65 (2014) 76–84, https://doi.org/10.1016/j.cemconres.2014.07.014.
[57] J. Shi, X. Guan, Chloride-induced corrosion of galvanized steel in ordinary Portland cement and alkali-activated fly ash mortars with benzotriazole, Cem. Concr. Compos 162 (2025) 106117, https://doi.org/10.1016/j.cemconcomp.2025.106117.
[58] E. Maahn, B. Sorensen, The influence of microstructure on the corrosion properties of hot-dip galvanized reinforcement in concrete, Corrosion 42 (1986) 187–196, https://doi.org/10.5006/1.3585996.